*Inorg. Chem.* **2004**, *43*, 3631–3641


# Alkaline Side-Coordination Strategy for the Design of Nickel(II) and Nickel(III) Bis(1,2-diselenolene) Complex Based Materials

**Xavi Ribas,[†] João C. Dias,[‡] Jorge Morgado,[‡,§] Klaus Wurst,[||] Isabel C. Santos,[‡] Manuel Almeida,[‡] José Vidal-Gancedo,[†] Jaume Veciana,[†] and Concepció Rovira*,[†]**

*Institut de Ciència de Materials de Barcelona, CSIC, Campus de la UAB, E-08193 Bellaterra, Spain, Departamento de Química, Instituto Tecnológico e Nuclear, P-2686-953 Sacavém, and Departamento de Engenharia Química, Instituto Superior Técnico, Av. Rovisco Pais, P-1049-001 Lisboa, Portugal, and Institut für Allgemeine Anorganische und Theoretische Chemie, Universitat Innsbruck, Innrain 52a, Innsbruck, Austria*

Received February 3, 2004

The deprotonated form of the pyrazine-2,3-diselenol (pds) ligand, $pds^{2-}$, reacts with $Ni^{II}$ inorganic salts to form the nickel compounds $[Ni^{II}(pds)_2](nBu_4N)_2$ (**1**), $[Ni^{II}(pds)_2]Na_2 \cdot 2H_2O$ (**2**), and $[Ni^{III}(pds)_2]_2Na_2 \cdot 4H_2O$ (**3**), depending on the reaction conditions. They are characterized by NMR, EPR, UV–vis, and IR spectroscopies, elemental analysis, cyclic voltammetry, and X-ray crystallography. The crystal structure of compound **3** shows the formation of segregated stacks of $Ni(pds)_2^-$ units, with a strong dimerization along the stacks. The stacked fashion of the crystal packing was expected since the supramolecular forces of the alkaline side coordination to the pyrazine moieties dominate, as happens in the recently reported analogous copper system $[Cu^{III}(pds)_2]Na \cdot 2H_2O$. The structure of **2** further emphasizes the alkaline coordination as the dominating supramolecular event, and an orthogonal array of 2D layers is observed. The absence of alkaline cations in complex **1** is reflected in a crystal packing with isolated complex $Ni(pds)_2^{2-}$ units. The dimerization found in the paramagnetic $Ni^{III}$ complex **3** promotes a very strong antiferromagnetic interaction, leading to a singlet ground state.

## Introduction

Bis(1,2-dithiolene) transition-metal complexes have been extensively studied due to their combination of functional properties, specific geometries, and intermolecular interactions that confer them an enormous interest in the field of conducting and magnetic materials, dyes, nonlinear optics, and others.[1] The electronically delocalized core comprising the central metal, four sulfurs, and the C=C units (see Chart 1a) accounts for a rich electrochemical behavior that often yields one or more reversible redox processes. In some materials such complexes show mixed-valence redox behavior as in the one-dimensional conductor $[Pt(mnt)_2]Li_{0.75} \cdot 2H_2O$ reported by Underhill et al.,[2] with a room-temperature conductivity $\sigma_{RT} = 30-200$ S cm$^{-1}$. But also neutral complexes lead to single-component molecular metals showing high electrical conductivities, highlighting $Ni(tmdt)_2$ ($\sigma_{RT} = 400$ S cm$^{-1}$),[3] $Cu(dmdt)_2$ ($\sigma_{RT} = 3$ S cm$^{-1}$),[4] $Au(\alpha\text{-tpdt})_2$ ($\sigma_{RT} = 6$ S cm$^{-1}$),[5] and $Au(tmdt)_2$ ($\sigma_{RT} = 15$ S cm$^{-1}$).[6] All these materials fulfill the requirements for the formation of

**Chart 1.** (a) General Formula for $[M(dithiolene)_2]^Y$ and (b) Formula of Monoanionic $Cu^{III}$ Complexes with Ligands pds (X = Se) and pdt (X = S)[10]

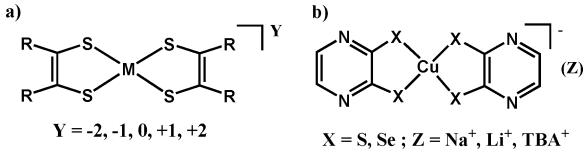


* Author to whom correspondence should be addressed. E-mail: cun@icmab.es. Fax: +34-935805729.
[†] CSIC.
[‡] Instituto Tecnológico e Nuclear.
[§] Instituto Superior Técnico.
[||] Universitat Innsbruck.

(1) Robertson, N.; Cronin, L. *Coord. Chem. Rev.* **2002**, *227*, 93−127.
(2) (a) Underhill, A. E.; Ahmad, M. M. *J. Chem. Soc., Chem. Commun.* **1981**, 67. (b) Kobayashi, A.; Sasaki, Y.; Kobayashi, H.; Underhill, A. E.; Ahmad, M. M. *J. Chem. Soc., Chem. Commun.* **1982**, 390.
(3) (a) Kobayashi, A.; Tanaka, H.; Kumasaki, M.; Torii, H.; Narymbetov, B.; Adachi, T. *J. Am. Chem. Soc.* **1999**, *121*, 10763-10771. (b) Tanaka, H.; Okano, Y.; Kobayashi, H.; Suzuki, W.; Kobayashi, A. *Science* **2001**, *291*, 285.
(4) Tanaka, H.; Kobayashi, H.; Kobayashi, A. *J. Am. Chem. Soc.* **2002**, *124*, 10002−10003.
(5) Belo, D.; Alves, H.; Lopes, E. B.; Duarte, M. T.; Gama, V.; Henriques, R. T.; Almeida, M.; Pérez-Benítez, A.; Rovira, C.; Veciana. J. *Chem.—Eur. J.* **2001**, *7*, 511−519.

10.1021/ic049860x CCC: $27.50 
Published on Web 05/15/2004

partially filled electronic bands, necessary to support metallic properties.[7] To accomplish these requirements, the use of crystal engineering tools becomes crucial to achieve the adequate packing of the molecules that may lead to the desired properties. Several approaches have been widely used, the main one being $\pi-\pi$ interactions between extended TTF-like compounds and chalcogen−chalcogen contacts to increase the dimensionality of the electronic interactions in these materials. Recently, Akutagawa and co-workers have controlled and tuned the crystal packing of $[Ni(dmit)_2]^-$ anions by using flexible supramolecular H-bonding from a set of *p*-xylylenediammonium−crown ether cations, thereby controlling their magnetic and electrical properties.[8] In our attempt to synthesize mixed-valence compounds such as the highly conducting unidimensional $[Pt(mnt)_2]Li_{0.75}\cdot 2H_2O$ complex,[2] we have very recently reported a supramolecular strategy consisting in the alkaline ion side coordination to control the crystal packing in a family of $Cu^{III}$ complexes with pyrazine-2,3-diselenolate ($pds^{2-}$) and pyrazine-2,3-dithiolate ($pdt^{2-}$) ligands, which show different 3D structures depending on the countercation used (see Chart 1b).[9,10] Namely, the use of alkaline cations leads to a stacked arrangement of $Cu^{III}$ complex units. In this paper we describe the synthesis of the analogue $Ni^{II}$ and $Ni^{III}$ complexes and their structural, electrical, and magnetic properties and discuss the oxidation states of the metal centers and ligands.[11]

## Experimental Section

**Materials.** Solvents of reagent grade quality supplied by SDS were dried before use by standard methodology, and stored under Ar. Reagents were obtained commercially from Aldrich and used without further purification.

Elemental analyses were performed by SA-UAB (Servei d'Anàlisi-Universitat Autònoma de Barcelona). UV−vis−near-IR spectra were recorded on a Varian Cary 5 spectrophotometer. NMR spectroscopy was performed on a Bruker DPX 250 MHz spectrometer. IR spectra were obtained on a Perkin-Elmer Spectrum One spectrophotometer using KBr pellets. Cyclic voltammetry (CV) experiments were carried out at room temperature with an EG&G (PAR263A) potentiostat−galvanostat in a normal three-electrode cell ($Ag/Ag^+$ reference) with Pt wires as working and auxiliary electrodes. Distilled and argon-degassed methanol and acetonitrile were used as solvents with $(n-Bu_4N)^+PF_6^-$ (0.1 M) as supporting electrolyte (scan rate 100 mV $s^{-1}$).

The ligand pyrazine-2,3-diselenol (pds) was synthesized following the method described in the literature.[12]

Caution! Perchlorate salts are potentially explosive and should be handled with care.

**$[Ni^{II}(pds)_2](n-Bu_4N)_2$ (1).** A 238.0 mg (1.0 mmol) sample of pds was dissolved in 10 mL of an aqueous solution of NaOH (1% w/w). A solution of 338.5 mg (1.05 mmol) of tetrabutylammonium bromide ($n-Bu_4NBr$) in 2 mL of $H_2O$ was added, followed by a solution of 123.6 mg (0.52 mmol) of $NiCl_2\cdot 6H_2O$ in 2 mL of $H_2O$, under an inert atmosphere. The mixture was then filtered and the precipitate leached with water. To remove the unreacted $Na_2(pds)$, the solid was dissolved in 15 mL of hot dichloromethane and filtered. The filtrate was then evaporated to dryness. The product was recrystallized in acetonitrile−water, giving red crystals of **1**. Yield: 45%. UV−vis ($CH_3CN$): $\lambda_{max}$/nm ($\epsilon/cm^{-1}\ M^{-1}$) = 341 (28000), 395 (sh, 10900), 462 (sh, 6000), 660 (sh, 3100), 795 (4900). IR (KBr pellet): $\nu/cm^{-1}$ = 2940, 1450, 1397, 1357, 1292, 1122, 1040, 1019, 875, 810, 730, 620. Anal. Calcd for $C_{40}H_{76}N_6Se_4Ni$: C, 47.30; H, 7.54; N, 8.27. Found: C, 46.84; H, 7.34; N, 8.10. CV (in $CH_3CN$): $E_{1/2}$ (vs Ag/AgCl) = −0.12 V.

**$[Ni^{II}(pds)_2]Na_2\cdot 2H_2O$ (2).** Into a suspension of pyrazine-2,3-diselenol (75 mg, 0.315 mmol) in 3.5 mL of $CH_3CN$ magnetically stirred under an Ar-controlled atmosphere was injected a NaOH(aq) (2 M) solution (0.47 mL, 0.95 mmol), causing the reaction mixture to change color from orange to yellow, and completely dissolving the suspended solid. After an additional 5 min of stirring, solid $Ni^{II}(ClO_4)_2\cdot 6H_2O$ (38.4 mg, 0.105 mmol) was added under Ar. The solution color turned intense red, and after 4 h of strong stirring, the solution was filtered through Celite. Diffusion of diethyl ether into the filtrated solution yielded pure **2** as red prism crystals (32 mg, 50.1%, 0.053 mmol). UV−vis ($CH_3CN$): $\lambda_{max}$/nm ($\epsilon/cm^{-1}\ M^{-1}$) = 334 (28300), 390 (sh, 6600), 480 (4500), 505 (4600), 797 (1900). UV−vis ($CH_3OH$): $\lambda_{max}$/nm ($\epsilon/cm^{-1}\ M^{-1}$) = 336 (31300), 400 (sh, 8200), 484 (4200), 798 (3600). IR (KBr pellet): $\nu/cm^{-1}$ = 3383, 2925, 1541, 1475, 1418, 1324, 1183, 1137, 1061, 841, 823, 547. Anal. Calcd for $C_8H_8N_4NiNa_2O_2Se_4$: C, 15.68; H, 1.32; N, 9.14. Found: C, 15.78; H, 1.16; N, 8.95. CV (in $CH_3CN$): $E_{1/2}$ (vs Ag/AgCl) = −0.16 V. CV (in $CH_3OH$): $E_{1/2}$ (vs Ag/AgCl) = −0.03 V.

**$[Ni^{III}(pds)_2]_2Na_2\cdot 4H_2O$ (3).** Into a magnetically stirred suspension of pyrazine-2,3-diselenol (50 mg; 0.21 mmol) in 3 mL of $CH_3CN$ was injected a NaOH(aq) (3 M) solution (0.21 mL, 0.63 mmol), causing the reaction mixture to change color from orange to yellow, and completely dissolving the suspended solid. After an additional 5 min of stirring, $Ni^{II}(ClO_4)_2\cdot 6H_2O$ (25.6 mg, 0.07 mmol) was added, and the solution color turned intense red. This solution was then exposed to an oxygen flow for 5 min followed by 4 h of strong stirring in contact with open air. The obtained red-brown solution was filtered through Celite. Slow diffusion of diethyl ether into the filtrated solution yielded crystals of **3** contaminated with red crystals of **2**. The higher solubility of **3** in acetone allowed the separation of both compounds. Final recrystallization from acetone/diethyl ether yielded black-brown block crystals of **3** (24 mg, 58.1%, 0.041 mmol). UV−vis ($CH_3CN$): $\lambda_{max}$/nm ($\epsilon/cm^{-1}\ M^{-1}$) = 335 (26200), 391 (8900), 460 (sh, 4600), 793 (4900). IR (KBr pellet): $\nu/cm^{-1}$ = 3504, 3454, 2923, 1534, 1462, 1403, 1316, 1144, 1135, 1055, 834, 636. Anal. Calcd for $C_8H_8N_4NiNaO_2Se_4$: C, 16.29; H, 1.37; N, 9.59. Found: C, 16.50; H, 1.38; N, 9.49. CV (in $CH_3CN$): $E_{1/2}$ (vs Ag/AgCl) = −0.16 V.

Compounds **1**−**3** were characterized by NMR, FT-IR, EPR, and UV−vis spectroscopy, elemental analysis, cyclic voltammetry, and X-ray diffraction studies.


(6) Suzuki, W.; Fujiwara, E.; Kobayashi, A.; Fujishiro, Y.; Nishibori, E.; Takata, M.; Sakata, M.; Fujiwara, H.; Kobayashi, H. *J. Am. Chem. Soc.* **2003**, *125*, 1486-1487.

(7) Kobayashi, A.; Tanaka, H.; Kobayashi, H. *J. Mater. Chem.* **2001**, *11*, 2078−2088.

(8) Akutagawa, T.; Hashimoto, A.; Nishihara, S.; Hasegawa, T.; Nakamura, T. *J. Phys. Chem. B* **2003**, *107*, 66−74.

(9) Ribas, X.; Dias, J.; Morgado, J.; Wurst, K.; Almeida, M.; Veciana, J.; Rovira, C. *Cryst. Eng. Commun.* **2002**, *4*, 564−567.

(10) Ribas, X.; Dias, J.; Morgado, J.; Wurst, K.; Molins, E.; Ruiz, E.; Almeida, M.; Veciana, J.; Rovira, C. *Chem.−Eur. J.* **2004**, *10*, 1691−1704.

(11) Chaudhuri, P.; Verani, C. N.; Bill, E.; Bothe, E.; Weyhermüller, T.; Wieghardt, K. *J. Am. Chem. Soc.* **2001**, *123*, 2213.

(12) (a) Papavassiliou, G. C.; Yiannopoulos, S. Y.; Zambounis, J. S. *Chem. Scr.* **1987**, *27*, 265−268. (b) Morgado, J.; Duarte, M. T.; Alcácer, L.; Santos, I. C.; Henriques, R. T.; Almeida, M. *Synth. Met.* **1997**, *86*, 2187−2188.

**Table 1.** Crystallographic Data for Compounds **1**−**3**

| | **1** | **2** | **3** |
|---|---|---|---|
| empirical formula | $C_{20}H_{38}N_3Ni_{0.50}Se_2$ | $C_8H_8N_4Na_2NiO_2Se_4$ | $C_{16}H_{16}N_8Na_2Ni_2O_4Se_8$ |
| fw | 507.81 | 612.71 | 1179.45 |
| $T$/K | 293(2) | 233(2) | 233(2) |
| $\lambda$/Å | 0.71073, Mo Kα | 0.71073, Mo Kα | 0.71073, Mo Kα |
| cryst syst | monoclinic | orthorhombic | monoclinic |
| space group | $P2_1/n$ | *Pbca* | $P2_1/c$ |
| $a$/Å | 8.2493(13) | 14.6372(4) | 7.5664(2) |
| $b$/Å | 20.3335(19) | 6.8642(2) | 12.5752(4) |
| $c$/Å | 14.238(3) | 15.5030(4) | 14.9926(5) |
| α/deg | 90 | 90 | 90 |
| $\beta$/deg | 99.382(15) | 90 | 91.094(2) |
| $\gamma$/deg | 90 | 90 | 90 |
| $V$/Å$^3$ | 2356.4(6) | 1557.63(7) | 1426.27(8) |
| Z | 4 | 4 | 2 |
| $\rho_{calcd}$/g cm$^{-3}$ | 1.431 | 2.613 | 2.746 |
| $\mu$/mm$^{-1}$ | 3.578 | 10.653 | 11.601 |
| no. of reflns collected | 5428 | 8369 | 16597 |
| no. of reflns with $I > 2\sigma(I)$ | 2037 | 1248 | 2235 |
| no. of independent params | 232 | 106 | 198 |
| $R(F_o)/R_w(F_o^2)$[a] | 0.0853/0.1263 | 0.0293/0.0751 | 0.0309/0.0764 |

[a] $R = \sum|F_o - F_c|/\sum F_o$ and $R_w = \{\sum[w(F_o^2 - F_c^2)^2]/\sum[w(F_o^2)^2]\}^{1/2}$, where $w = 1/[\sigma^2(F_o^2 + (aP)^2 + bP]$, $P = (F_o^2 + 2F_c^2)/3$, and $a$ and $b$ are constants given in the Supporting Information.

**X-ray Crystallography.** X-ray-quality crystals were grown by recrystallization in EtOH for complex **1**, and in $CH_3CN$/diethyl ether for complexes **2** and **3**. Crystal data for a red crystal of **1** were collected on an Enraf Nonius CAD4 diffractometer at 293(2) K equipped with graphite-monochromatized Mo Kα radiation ($\lambda$ = 0.71073 Å) in the $\omega-2\theta$ scan mode. X-ray diffraction data were collected at room temperature, and an empirical absorption correction based on a $\psi$ scan was applied. The structure was solved by direct methods using SIR97[13] and refined by full-matrix least-squares methods using the program SHELXL97[14] and the WinGX software package.[15] All non-hydrogen atoms were refined anisotropically. Hydrogen atoms were placed in calculated positions. Molecular graphics were prepared by using ORTEPIII.[16]

Data collection of red and black crystals of **2** and **3**, respectively, was performed on a Nonius Kappa CCD diffractometer with graphite-monochromated Mo Kα radiation ($\lambda$ = 0.71073 Å) at 233(2) K.

Intensities were integrated using DENZO and scaled with SCALEPACK. Several scans in the $\phi$ and $\omega$ directions were made to increase the number of redundant reflections, which were averaged in the refinement cycles. This procedure replaces an empirical absorption correction. The structure was solved with direct methods (SHELXS86) and refined against $F^2$ (SHELX97).[14] Hydrogen atoms at carbon atoms were added geometrically and refined using a riding model. Hydrogen atoms of the water molecules were refined with isotropic displacement parameters. All non-hydrogen atoms were refined with anisotropic displacement parameters.

Further details of the crystal structure determinations are given in Table 1. Graphical representations were prepared using the ORTEPIII[16] and Mercury 1.1 (CCDC) programs.

**Electrical and Magnetic Characterization.** The electrical resistivity was measured along the long axis of selected single crystals of compound **3** placed in a cell attached to the cold stage of a closed-cycle helium refrigerator. Thin $\phi$ = 25 $\mu$m gold wires were directly attached to the sample with platinum paint to achieve a four-in-line contact geometry, and measurements were made applying an ac current of 1 $\mu$A at 77 Hz, the voltage being measured by a lock-in amplifier (EG&G Par 5316).[17,18] The samples were previously checked for unnested/nested voltage ratio,[19] which was kept below 5%.

EPR spectra of **2** and **3** were obtained in a conventional X-band spectrometer (Bruker ESP 300 E) equipped with a microwave bridge ER041XK, a rectangular cavity operating in T102 mode, a field frequency lock ER 033M, and a Bruker variable-temperature unit, which enabled measurements in the temperature range 77−350 K. The measurements were performed on a bulk polycrystalline sample, placed inside a quartz tube. The modulation amplitude was kept well below the line width and the microwave power well below saturation.

The static magnetic susceptibility of a polycrystalline randomly oriented sample of **3** was measured in the temperature range 2−300 K using a Faraday system (Oxford Instruments) equipped with a 7 T superconducting magnet. The measurements were performed under a static magnetic field of 2 T. The force on the samples, contained in a previously measured thin-walled Teflon bucket, was measured with a microbalance (Sartorius S3D-V) applying forward and reverse gradients of 1 T/m. The paramagnetic susceptibility was calculated considering a diamagnetic correction, estimated from tabulated Pascal constants.

## Results and Discussion

**Synthesis.** The new $Ni^{II}$ complexes with the ligand pds[12] were obtained following known procedures. Complex **1** was isolated by precipitation from a water solution after the addition of $n$Bu$_4$NBr.[20] The $Ni^{II}$ complex **2** was synthesized by a procedure similar to that used in the preparation of the

(13) Altomare, A.; Burla, M. C.; Camalli, M.; Cascarano, G.; Giacovazzo, G.; Guagliardi, A.; Moliterni, A. G. G.; Polidori G.; Spagna, R. *J. Appl. Crystallogr.* **1999**, *32*, 115−119.
(14) Sheldrick, G. M. *SHELXL97: Program for the Refinement of Crystal Structures*; University of Göttingen: Göttingen, Germany, 1997.
(15) Farrugia, L. J. *J. Appl. Crystallogr.* **1999**, *32*, 837−838.
(16) (a) ORTEP3 for Windows: Farrugia, L. J. *J. Appl. Crystallogr.* **1997**, *30*, 565. (b) McArdle, P. *J. Appl. Crystallogr.* **1995**, *28*, 65.
(17) Lopes, E. B. ITN Internal Report, 1991.
(18) Chaikin, P. M.; Kwak, J. F. *Rev. Sci. Instrum.* **1975**, *46*, 218.
(19) Schaffer, P. E.; Wudl, F.; Tomas, G. A.; Ferraris, J. P.; Cowen, D. O. *Solid State Commun.* **1974**, *14*, 347.
(20) Simão, D.; Alves, H.; Belo, D.; Rabaça, S.; Lopes, E. B.; Santos, I. C.; Gama, V.; Duarte, M. T.; Henriques, R. T.; Novais, H.; Almeida, M. *Eur. J. Inorg. Chem.* **2001**, 3119−3126.

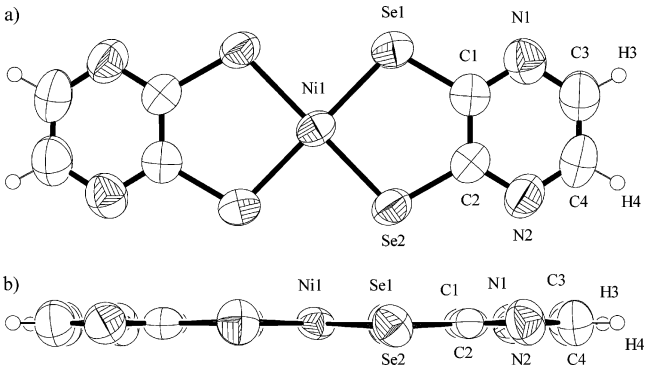


**Figure 1.** ORTEP drawing of the dianion $[Ni^{II}(pds)_2]^{2-}$ in **1** in views perpendicular (a) and parallel (b) to the molecular plane.

**Table 2.** Selected Bond Lengths (Å) and Angles (deg) for Complex **1**

| | | | |
|---|---|---|---|
| Ni1−Se1 | 2.2955(9) | Se1−C1 | 1.874(8) |
| Ni1−Se2 | 2.2839(9) | Se2−C2 | 1.883(8) |
| Ni1···Ni1′ | 8.2493(13) | | |
| Se1−Ni1−Se1′ | 180.0 | Se1−C1−C2−N2 | 179.3(1) |
| Se2−Ni1−Se2′ | 180.0 | Se2−C2−C1−N1 | 178.0(1) |
| Se1−Ni1−Se2′ | 91.84(3) | N1−C1−Se1−Ni1 | 179.8(1) |
| Se1−Ni1−Se2′ | 88.16(3) | N2−C2−Se2−Ni1 | −177.7(1) |
| Se1−Ni1−Se2′−C2′ | −177.5(1) | | |
| Se2−Ni1−Se1′−C1′ | 177.8(1) | | |

analogue $[Cu^{III}(pds)_2]^-$ complexes recently reported,[9,10] but working in an $O_2$-free atmosphere to prevent oxidation. The alkaline salt of the $Ni^{III}$ complex **3** was obtained by air oxidation of **2**.

**Crystal Structures**. The crystal structure of the $Ni^{II}$ complex **1** was solved at 293(2) K, whereas those of complexes **2** and **3** were solved at 233(2) K. Crystal and refinement data for all three compounds are given in Table 1.

**$[Ni^{II}(pds)_2](nBu_4N)_2$ (1).** The asymmetric unit of **1** contains half a pds ligand and one $nBu_4N$ cation in general positions, and half a Ni atom located at a symmetry center. The ORTEP plot of the anionic fragment $[Ni^{II}(pds)_2]^{2-}$ depicted in Figure 1 shows a square-planar geometry around the Ni center, with Ni−Se bond distances close to 2.29 Å. Differently from the isoelectronic $Cu^{III}$ analogue complex $[Cu^{III}(pds)_2](nBu_4N)$,[10] no significant distortion in the planarity is observed (see Table 2).

The unit cell contains two $[Ni(pds)_2]^{2-}$ units. The long axis of the unit centered in the center of the unit cell is tilted by ∼30° with respect to the long axis of the units located at the vertexes (see Figure 2). The formation of layers is precluded due to the presence of two $nBu_4N$ cations per $[Ni(pds)_2]^{2-}$ anionic complex, which isolate the dianions, preventing any contact between them. This effective isolation may favor the stabilization of the expected square-planar geometry for a $Ni^{II}$ with a $d^8$ electronic configuration.

**$[Ni^{II}(pds)_2]Na_2\cdot 2H_2O$ (2).** The asymmetric unit of **2** contains one pds ligand, one water molecule, and one Na atom in general positions, and one Ni atom in a special position, located in a symmetry center. The ORTEP plot of the dianionic fragment $[Ni^{II}(pds)_2]^{2-}$, depicted in Figure 3, shows a square-planar geometry around the Ni, with Ni−Se bond distances close to 2.30 Å. However, as shown in Figure 3b, a small distortion is observed in the planarity of the whole complex, with both the pyrazine rings being twisted in the same direction (boat distortion) with respect to the $NiSe_4$ plane (torsion angle N−C−Se−Ni ≈ 174°). This deviation from planarity can be explained by the coordination of the nitrogen atoms of the pyrazine rings with the $Na^+$ counterions, similarly but more pronounced than in the isoelectronic analogue copper complex $[Cu^{III}(pds)_2]Na\cdot 2H_2O$.[9] Selected bond distances and angles are listed in Table 3.

**$[Ni^{III}(pds)_2]_2Na_2\cdot 4H_2O$ (3).** X-ray diffraction of a black-brown block single crystal of **3** (see Table 1 for crystal data) shows a strong dimerization of the $Ni(pds)_2$ units. Within a dimer, these units are related by a center of symmetry and connected by two Ni−Se bonds. Consequently, each Ni center is coordinated to four Se atoms of the same unit and one Se of the other unit, defining a square-pyramidal geometry.

The asymmetric unit contains one $Ni(pds)_2$ fragment, one Na atom, and two water molecules in general positions. The ORTEP plot of the dimeric dianion $[Ni^{III}(pds)_2]_2^{2-}$ depicted in Figure 4 shows the two fragments in a chair conformation determined by the strong intradimer Ni−Se bonds of 2.49 Å. Within each $Ni(pds)_2$ fragment the Ni−Se bond lengths are in the range 2.30−2.33 Å, with bond angles clearly distorted from the square-planar geometry as listed in Table 4. Indeed, the Ni atoms are 0.299 Å above the centroid defined by the four Se atoms of each $Ni(pds)_2$ unit. The pyrazine residues of the pds ligands of the same $Ni(pds)_2$ anionic complex are not coplanar due to the strong dimerization. They are twisted with respect to each other, due to the coordination of one of the nitrogen atoms of the pyrazine rings with the $Na^+$ counterion (a similar effect is observed in the copper complex $[Cu^{III}(pds)_2]Na\cdot 2H_2O$).[9] Relevant bond distances and angles are listed in Table 4.

As shown in Figure 5, the unit cell contains two $[Ni^{III}(pds)_2]_2^{2-}$ dimeric units with their long axes almost perpendicular to each other. These anionic complexes form stacks along the *a* axis, with an angle between the stacking axis *a* and the average $Ni(pds)_2$ plane of 24°. The average distance between aromatic planes (i.e., the distance between centroids defined by the pyrazine rings) within the dimer is 3.746 Å, with the shortest contact being N3···C2 (3.377 Å), whereas between dimers the interaromatic centroid distance is 3.933 Å, with the shortest contact being C4···C8 (3.670 Å).

The dimerization observed was not completely unexpected since other dimeric $Ni^{III}$ complexes with diselenolene and dithiolene ligands have been reported. Particularly similar is the $[Ni(dsit)_2]_2(nBu_4N)_2$ complex (dsit = 1,3-dithiole-2-thione-4,5-diselenolate),[21] with an analogous dimeric structure having only slightly longer basal Ni−Se bond distances. The structure of **3** is also similar to that of the reported dimerized bis(dithiolene) compound $[Ni(dcbdt)_2]_2(nBu_4N)_2$ (dcbdt = 4,5-dicyanobenzene-1,2-dithiolate),[20] with compa-

(21) Cornelissen, J. P.; Haasnoot, J. G.; Reedijk, J.; Faulmann, C.; Legros, J.-P.; Cassoux, P.; Nigrey, P. J. *Inorg. Chim. Acta* **1992**, *202*, 131−139.

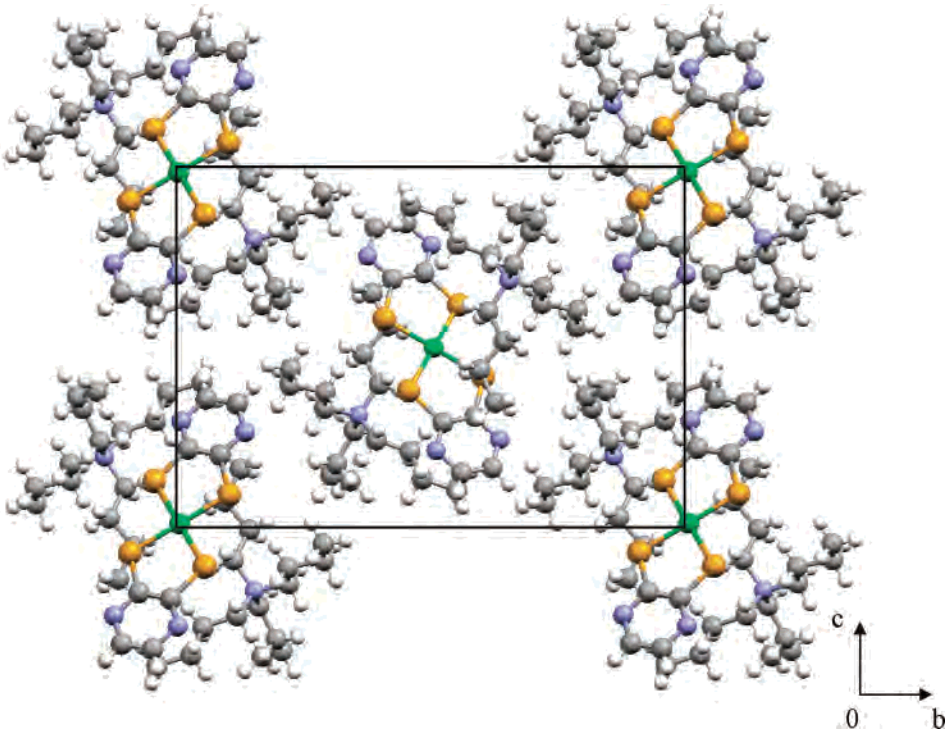


**Figure 2.** Crystal structure of **1** in a view along the *a* axis.

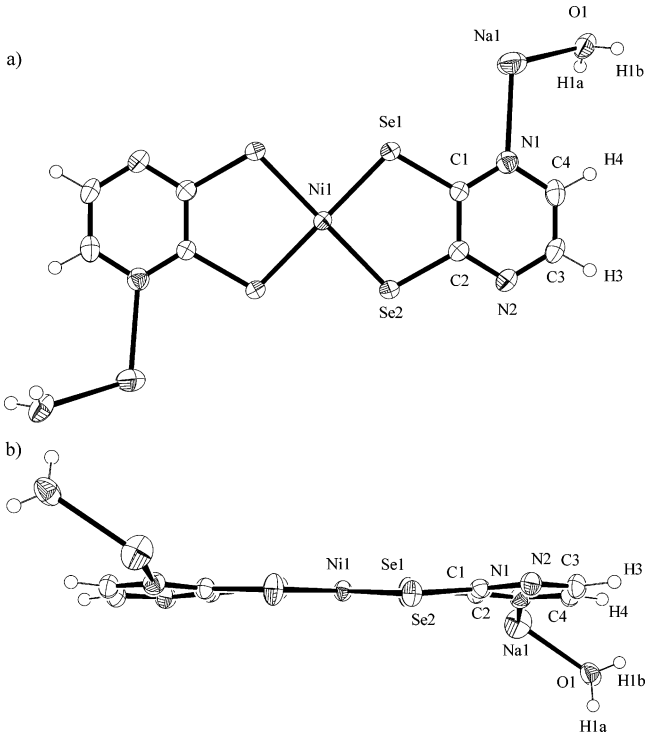


**Figure 3.** ORTEP plot of compound $[Ni^{II}(pds)_2)]Na_2{\cdot}2H_2O$ (**2**) in views perpendicular (a) and parallel (b) to the molecular plane.

rable bond distances taking into account the different atomic radius of the chalcogen atom.

**Supramolecular Role of the Sodium Ion**. The packing motives observed in **3** are very similar to those found in the structure of $[Cu^{III}(pds)_2]Na{\cdot}2H_2O$,[9] the main difference being the clear dimerization of the anionic complex units in **3**, along the stacking axis. As in the $Cu^{III}$ analogue, each Na ion is coordinated to two N atoms belonging to the two $[Ni^{III}(pds)_2]$ units with parallel orientation, and four O atoms from water molecules (see Figure 6a and Table 4). In this way, one-dimensional chains of alternating Na ions and two water molecules are formed along *a*, between the stacks of $[Ni^{III}(pds)_2]_2^{2-}$ dimers. However, due to the dimerization of the $Ni(pds)_2^-$ units, the Na···Na distance alternates between 3.82 and 3.77 Å (Figure 5c), the larger distance being between two Na ions bridging the same two dimers. The supramolecular motif formed by the sodium cations and water molecules can be described as an infinite chain of $\cdots Na-(\mu\text{-}O_{aq})_2-Na-(\mu\text{-}O_{aq})_2\cdots$ as depicted in Figures 5c and 6b, and defined as monodimensional supramolecular beams that dominate and stabilize the 3D structure of the complex.

**Table 3.** Selected Bond Lengths (Å) and Angles (deg) for Complex **2**

| | | | |
|---|---|---|---|
| Ni1−Se1 | 2.2983(4) | Ni1···Na1 | 3.2600(18) |
| Ni1−Se2 | 2.3019(4) | Na1···Na1′ | 3.374(3) |
| Se1−C1 | 1.894(3) | Ni1···Ni1′ | 6.8642(2) |
| Se2−C2 | 1.895(3) | Na1···Se1 | 3.5207(18) |
| Na1−N1 | 2.396(3) | Na1···Se2 | 3.4679(18) |
| Na1−O1 | 2.338(3) | O1···O1′ | 3.256(6) |
| Na1−O1′ | 2.350(4) | | |
| Se1−Ni1−Se1′ | 180 | Se1−Ni1−Se2′−C2′ | −175.3(1) |
| Se2−Ni1−Se2′ | 180 | Se2−Ni1−Se1′−C1′ | 178.9(1) |
| Se1−Ni1−Se2 | 92.274(11) | Se1−C1−C2−N2 | 173.5(2) |
| Se2−Ni1−Se1′ | 87.726(11) | Se2−C2−C1−N1 | 170.3(2) |
| Na1−O1−Na1 | 92.04(11) | N1−C1−Se1−Ni1 | −175.3(2) |
| O1−Na1−O1 | 87.96(11) | N2−C2−Se2−Ni1 | −173.8(2) |
| N1−Na1−O1 | 158.36(14) | N1−Na1−O1−Na1′ | 150.0(3) |
| N1−Na1−O1′ | 110.61(12) | | |

Several Ni bis(dichalcogenene) complexes have been reported in the literature, all of them with a 3D structure mostly unpredictable. On the contrary, the structure of compound **3** is found to be as expected taking into account the recently reported work on the $pds^{2-}$ ligand[9,10] about the formation of segregated stacks of complex anions due to the

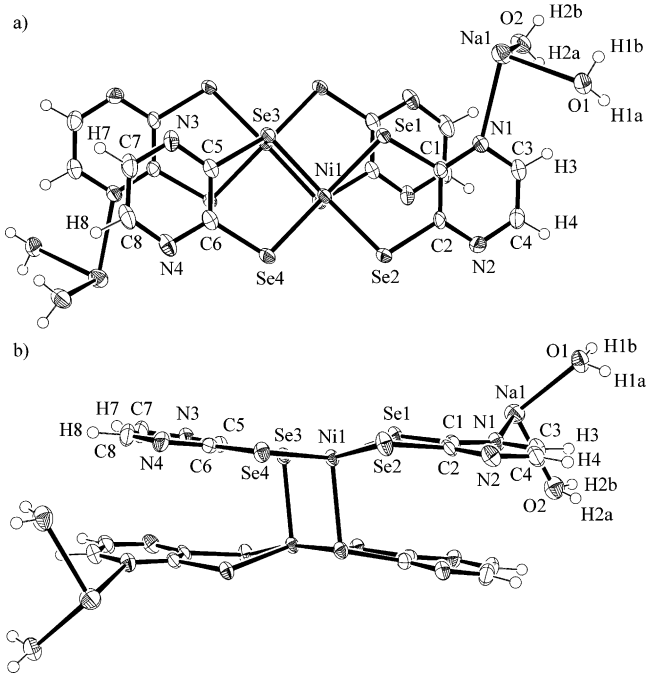


**Figure 4.** ORTEP plot of the dimeric compound $[Ni^{III}(pds)_2)]_2Na_2{\cdot}4H_2O$ (**3**) in perpendicular (a) and parallel (b) views to the $NiSe_4$ planes. The two fragments of the dimer are equivalent.

**Table 4.** Selected Bond Lengths (Å) and Angles (deg) for Complex **3**

| | | | |
|---|---|---|---|
| Ni1−Se1 | 2.3288(7) | Na1−N1 | 2.603(4) |
| Ni1−Se2 | 2.3200(7) | Na1′−N4 | 2.663(5) |
| Ni1−Se3 | 2.2955(6) | Na1−O1 | 2.506(4) |
| Ni1−Se4 | 2.3243(7) | Na1−O2 | 2.453(4) |
| Ni1−Se3′ | 2.4902(7) | Na1−O1′ | 2.502(4) |
| Se1−C1 | 1.896(4) | Na1−O2′ | 2.610(4) |
| Se2−C2 | 1.877(5) | Na1···Na1′ [a] | 3.817(4) |
| Se3−C5 | 1.901(5) | Na1···Na1′ [b] | 3.769(4) |
| Se4−C6 | 1.876(5) | Ni1···Ni1′ | 3.182(1) |
| Se1−Ni1−Se2 | 90.19(2) | Na1−O1−Na1′ | 97.61(13) |
| Se1−Ni1−Se3 | 86.48(2) | Na1−O2−Na1′ | 97.80(15) |
| Se2−Ni1−Se4 | 87.75(2) | Na1−O1′−Na1′ | 97.61(13) |
| Se3−Ni1−Se4 | 92.13(2) | Na1−O2′−Na1′ | 97.80(15) |
| Se1−Ni1−Se4 | 160.66(3) | Na1···Na1′···Na1 | 171.87(12) |
| Se2−Ni1−Se3 | 169.60(3) | Se1−Ni1−Se3−C5 | 154.6(1) |
| Ni1−Se3−Ni1′ | 83.23(2) | Se1−Ni1−Se4−C6 | −82.0(2) |
| Se3−Ni1−Se3′ | 96.77(2) | Se2−Ni1−Se3−C5 | 83.1(2) |
| Se1−Ni1−Se3′ | 103.00(3) | Se2−Ni1−Se4−C6 | −166.1(1) |
| Se2−Ni1−Se3′ | 93.58(3) | Se3−Ni1−Se1−C1 | 170.1(1) |
| Se4−Ni1−Se3′ | 96.33(2) | Se3−Ni1−Se2−C2 | 92.2(2) |
| N1−Na1−N4′ | 173.00(15) | Se4−Ni1−Se1−C1 | −103.5(2) |
| N1−Na1−O1 | 87.25(13) | Se4−Ni1−Se2−C2 | −178.3(1) |
| N1−Na1−O1′ | 83.74(14) | Se1−Ni1−Se3−Ni1′ | −102.7(1) |
| N1−Na1−O2 | 90.06(14) | Se2−Ni1−Se3−Ni1′ | −174.3(2) |
| N1−Na1−O2′ | 94.31(14) | Se4−Ni1−Se3−Ni1′ | 96.6(1) |
| O1−Na1−O1′ | 82.39(14) | Se1−Ni1−Se3′−Ni1′ | 87.9(1) |
| O1−Na1−O2 | 103.85(14) | Se2−Ni1−Se3′−Ni1′ | 179.0(1) |
| O1′−Na1−O2 | 171.02(15) | Se3−Ni1−Se3′−Ni1′ | 0 |
| O1′−Na1−O2′ | 91.77(13) | Se4−Ni1−Se3′−Ni1′ | −92.9(1) |

[a] Intradimer. [b] Interdimer.

presence of an alkaline−pyrazine side coordination that allows the formation of supramolecular 1D Na/water chains. The dominating supramolecular driving force to obtain such a structure is mainly attributed to the formation of the above-mentioned Na/water chains. These chains are clearly absent in the structure of **1**, in agreement with what was observed for the $(n\text{Bu}_4\text{N})^+$ salts of the $Cu^{III}$ analogues,[10] and other monoanionic bis(diselenolene) salts such as $[Ni(ddds)_2](R_4N)$ (ddds = 5,6-dihydro-1,4-dithiin-2,3-diselenolate; R = Me, Et, *n*Bu)[22] or $[Ni(dsise)_2](n\text{Bu}_4\text{N})$ (dsise = 1,3-dithiole-2-selenone-4,5-diselenolate).[23]

The formation of $\pi$-stacking is also prevented by the bulky $(n\text{Bu}_4\text{N})^+$ counteractions in the salts containing dimerized complexes such as $[Ni(dsit)_2]_2(n\text{Bu}_4\text{N})_2$ [21] and $[Ni(dcbdt)_2]_2$-$(n\text{Bu}_4\text{N})_2$.[20] In the last compound, a lateral chalcogen−chalcogen network is favored in front of the formation of stacked columns of dimers, as also occurs in the neutral compound $[Ni(ddds)_2]_2$.[22] The $\pi-\pi$ interaction between dimers along the stacks in **3** is relatively weak, and therefore, without the alkaline-mediated side coordination the dimers would probably not stack, which highlights the importance of this crystal engineering strategy.

On the other hand, the structure of **2** presents similarities with that of the $[Cu^{III}(pds)_2]Na{\cdot}2H_2O$ complex and also with that of compound **3** (vide supra), in the sense that the coordination of the sodium countercations is again dominating the supramolecular interactions and thus the 3D crystal packing. As seen in Figure 7a, the unit cell contains four $[Ni^{II}(pds)_2]^{2-}$ units with their long axes almost perpendicular to each other. Very interestingly in this structure, the sodium−water coordination system is also operative, but differently, in complex **2** there are two Na atoms per complex dianion, each one coordinated to one parallel complex unit, and both bridged by two water molecules (see Figure 7b). This imposes a larger separation between parallel anionic complex units (N···N = 7.94 Å in **2** compared with 5.26 Å in **3**), and as a consequence, the long axis of one unit is aligned with the Ni-centered short axis of the adjacent unit, with Se···H−C contacts that stabilize this packing motive. Apart from this variation, the packing motive within this 2D layer is similar to that found in compounds $[Cu^{III}(pds)_2]Na{\cdot}2H_2O$[9] and **3**. Also noticeable is the presence of two strong hydrogen bonds between each complex dianion and the water molecules (N2···H1b−O1, 2.034 Å, 162°), which further enhance the intralayer stabilization. The most significant differences arise from the packing along the *b* axis (notice here that the crystal cell has changed from monoclinic for **3** to orthorhombic for **2**, and the stacking axis for **3** is *a* whereas for **2** it is *b*; see Table 1).

The bridging water molecules between Na ions abort the possibility of forming the supramolecular Na/water chains as in $[Cu^{III}(pds)_2]Na{\cdot}2H_2O$[9] and **3**, and thus, the crystallographic relation between two layers consists of a rotation of 180° (by a 2-fold screw axis) followed by a movement of half lattice constant in the direction of the *c* axis. This rotation between layers results in a perpendicular superposition of complexes of different layers, as depicted in Figure 7a, further helped by the $\pi-\pi$ interaction between aromatic rings (interaromatic centroid distance of 3.651 Å, with the shortest distance being N2···C4′ = 3.290 Å). The reason for this rotation is probably the coordination demands of the sodium cations: each sodium is coordinated to one N atom

(22) Fujiwara, H.; Ojima, E.; Kobayashi, H.; Courcet, T.; Malfant, I.; Cassoux, P. *Eur. J. Inorg. Chem.* **1998**, 1631−1639.
(23) Olk, R.-M.; Olk, B.; Rohloff, J.; Reinhold: J.; Sieler, J.; Trübenbach, K.; Kirmse, R.; Hoyer, E. *Z. Anorg. Allg. Chem.* **1992**, *609*, 103.

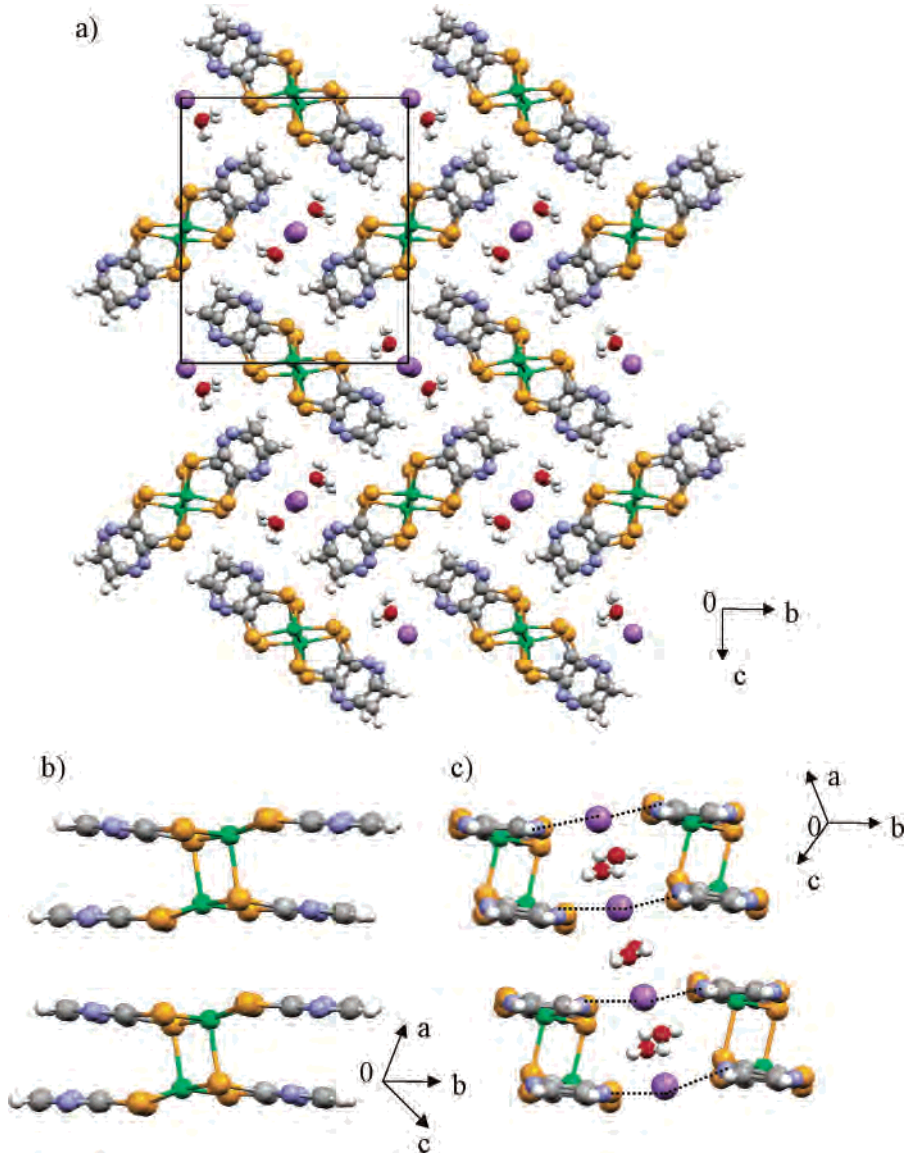


**Figure 5.** Crystal structure of **3**: (a) view along the stacking axis *a*; (b) stack of dimeric units viewed along the shortest axis of the molecule; (c) parallel stacks of dimer dianions viewed along the longest axis and connected through Na coordination.

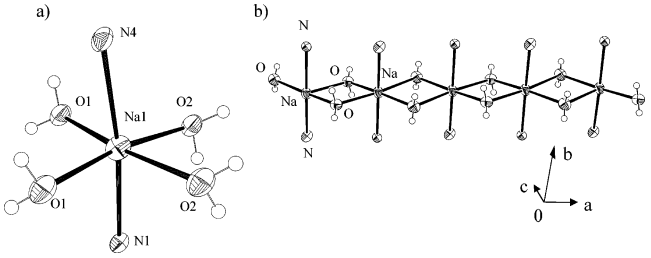


**Figure 6.** (a) Octahedral $N_2O_4$ coordination environment of Na centers of compound **3** and (b) infinite chain of $\cdots Na-(\mu\text{-}O_{aq})_2-Na-(\mu\text{-}O_{aq})_2\cdots$ atoms along the molecular stacking axis *a*.

and two water molecules with strong coordination bonds (<2.35 Å) in a distorted T-shaped planar geometry, but they increase the coordination number up to 9 with four Na···Se contacts (~3.5 Å), one Na···Na contact of 3.37 Å, and even one Na···Ni contact of 3.26 Å (see Figure 8).

The structure of **2** is a step forward in the understanding of the possibilities of the alkaline−pyrazine side-coordination system, and it is well compared with the related monocationic species **3**. The $Ni^{II}$ system has structurally resolved the situation of fitting two sodium ions per molecule in the 3D framework by the formation of comparable 2D layers but with an orthogonal array between them. Nevertheless, the Na ion coordination demands are again dominating the supramolecular 3D arrangement of compound **2**, as in the structurally related Cu−pds systems[9,10] and the $Ni^{III}$ complex **3**.

Further structural details related to the H-bond network also observed in structures **1**−**3** are described in the Supporting Information.

**Oxidation State of the Ni Ion.** Concerning the oxidation state of the complexes, there are no clear differences in the bond lengths of the $Ni(pds)_2$ anionic complexes in these three compounds. However, while the geometry around the metal center is square-planar for the $Ni^{II}$ complexes **1** and **2**, it is five-coordinated square-pyramidal in the $Ni^{III}$ complex **3** (with the Ni atom out of the plane formed by the four Se atoms that form the base of the pyramid) (see Tables 2−4).

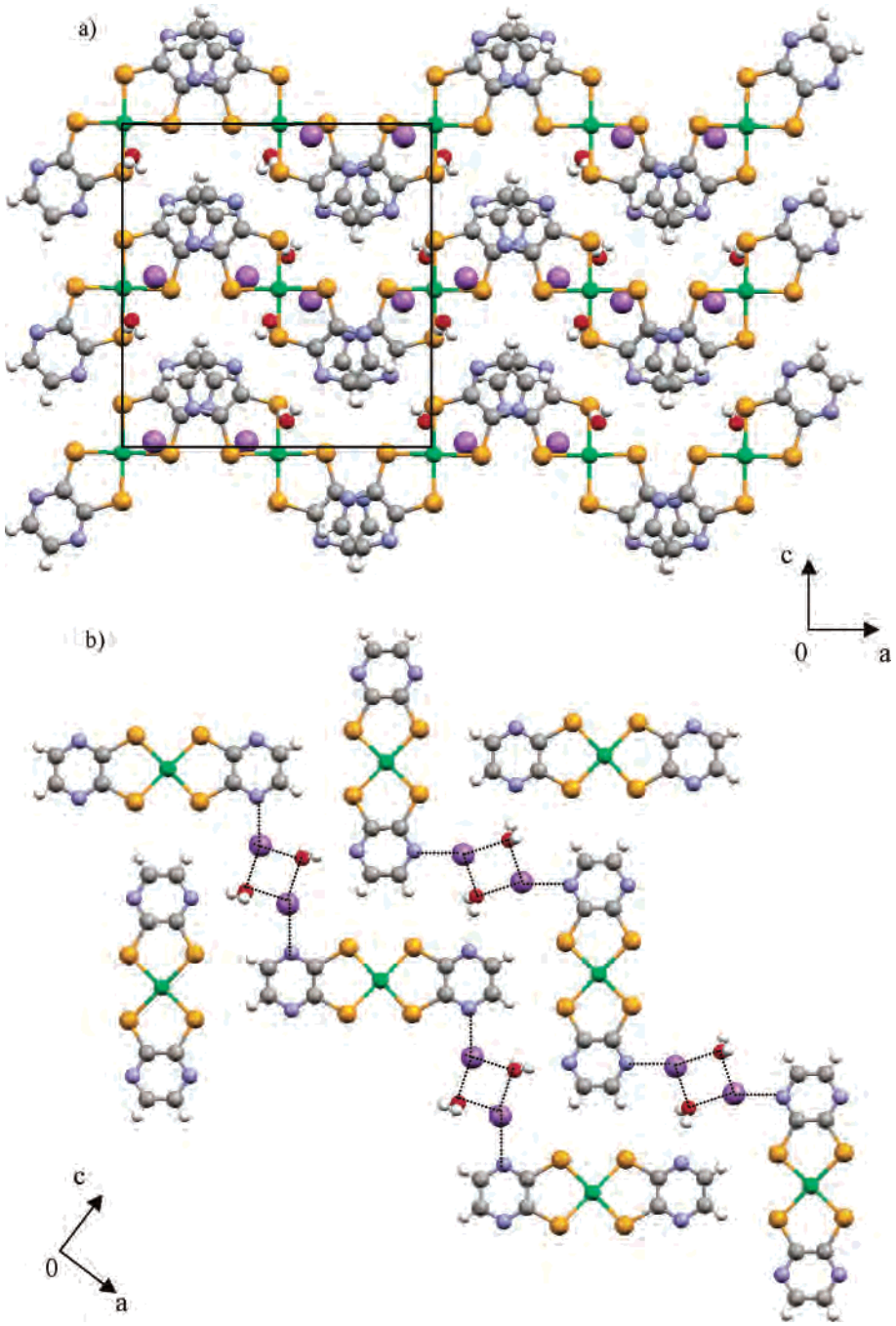


**Figure 7.** Crystal structure of **2**: (a) view along the *b* axis; (b) view of one 2D layer (dotted lines indicate the N−sodium−water supramolecular network).

From accurate XRD data, the aromatic (pyrazine) rings remain unaffected by a short−long−short C−C distance pattern as would appear for an *o*-semiquinonate-type ligand,[11] neither observed in the $[Cu(pds)_2]^-$ analogue.[10] The average value of the Se−C bond lengths is 1.879 Å for **1**, 1.895 Å for **2**, and 1.888 Å for **3**, also pointing toward a closed-shell configuration of the aromatic ligand. However, the Ni−Se bond distances enlarge when the $Ni^{II}$ salt **2** (Ni−Se ≈ 2.300 Å) is oxidized to the $Ni^{III}$ salt **3** (Ni−Se ≈ 2.317 Å), contrary to the normal trend of shorter M−L distances for higher oxidation states of the metal. This can be explained by the fact that there is a change of the geometry around the metal center in going from **2** to **3**; thus, the Ni−Se distance is not a comparable probe in this case. Therefore, we may conclude that the oxidation is mainly metal-centered, as the coordination geometry switches from square-planar ($Ni^{II}$-$d^8$) in **2** to square-pyramidal ($Ni^{III}$-$d^7$) in **3**. These oxidation states are also confirmed by EPR measurements (see the next section).

**Spectroscopic and Electronic Characterization.** The comparison of IR spectra of the alkaline salts **2** and **3** shows a slight shift to lower wavenumbers of all peaks for the $Ni^{III}$ complex **3**. In addition, only one peak of coordinated water is observed for **2** at 3383 $cm^{-1}$, but two peaks appear at 3504 and 3454 $cm^{-1}$ for **3**, indicating two distinguishable water molecules for the latter, accounting for the consequences of the observed dimerization (see the structural description above).

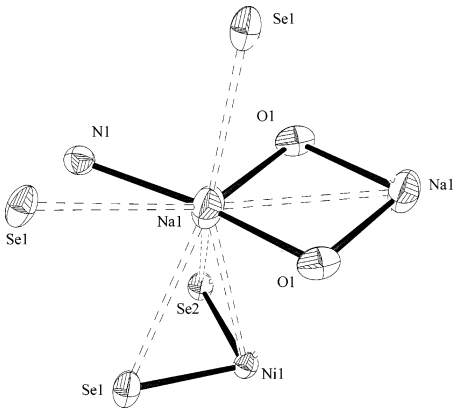


**Figure 8.** ORTEP diagram of the Na coordination environment in **2**.

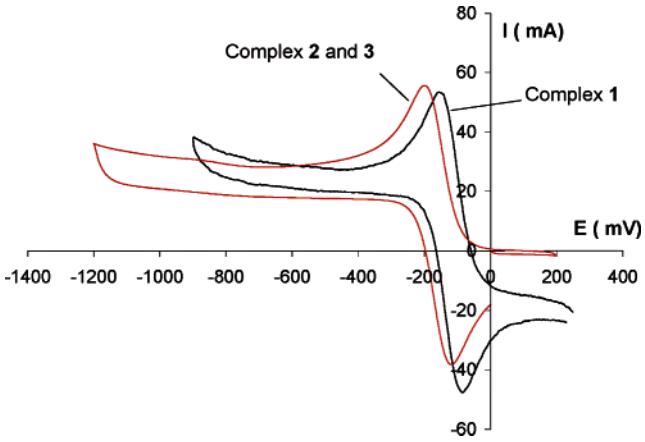


**Figure 9.** Cyclic voltammograms for $Ni^{II}$ compounds **1** and **2** and $Ni^{III}$ compound **3**. ($CH_3CN$, room temperature, $n$Bu$_4$NPF$_6$ (0.1 M), scan rate 100 mV/s).

As detailed in the Experimental Section, compound **2** only undergoes slow oxidation toward compound **3** under strong stirring in contact with $O_2$. Therefore, the characterization of **2** in solution is possible and decomposition neglected by working in a controlled Ar atmosphere.

Electronic spectra of $Ni^{II}$ complexes **1** and **2** in $CH_3CN$ show characteristic bands at 395, 462, 660, and 795 nm for **1** ($\epsilon$ = 10900, 6000, 3100, and 4900 $M^{-1}$ $cm^{-1}$, respectively) and at 480, 505, and 800 nm for **2** ($\epsilon$ = 4500, 4600, and 1900 $M^{-1}$ $cm^{-1}$, respectively), conferring the intense red-orange color to their solutions. For complex **2**, a solvatochromic effect is observed when the complex is dissolved in MeOH, doubling the intensity of the 800 nm ($\epsilon$ = 3600) band and showing the disappearance of the 505 nm band, with a resulting red-pink color of the methanolic solution. The electronic spectrum of **3** in acetonitrile does not show any band in the 480−700 nm region and, similarly to the spectra of **1** and **2**, presents a band at 793 nm ($\epsilon$ = 4900). The influence of the alkaline cation coordination on the extinction coefficients is reflected in the higher intensity of the band at 796 nm for **1** than for **2**. The low-energy band centered at 800 nm is characteristic of bis(dithiolene)nickel complexes and is usually assigned to a $\pi \rightarrow \pi^*$ transition between the HOMO and the LUMO. It usually appears as a broad but intense ($\epsilon$ = 15000−40000 $cm^{-1}$ $M^{-1}$) electronic transition, importantly related to the development of near-IR dyes,[24] which in turn are very important in Q-switching infrared lasers.[25] However, in the case of the bis(diselenolene)nickel complexes **1**−**3**, even though the $\pi \rightarrow \pi^*$ transition band is centered at low energy (800 nm), it is not an intense transition ($\epsilon$ values are lower than 5000 $cm^{-1}$ $M^{-1}$) in comparison to that of bis(dithiolene)nickel complexes. Since one of the conditions required to obtain high $\epsilon$ values, i.e., the coplanarity of the ligand, is fulfilled, the intensity of the transition should be affected by the substitution of S for Se. The change of chalcogen atom may have perturbed the $\pi$ symmetry of the frontier orbitals, as was demonstrated by DFT calculation on the analogue $[Cu(pds)_2]^-$ compounds.[10] For the latter species, an increased participation of $\sigma$-type Se and metal orbitals on the LUMO compared to that of the usual bis(dithiolene) $\pi$-type frontier orbitals[26] has been observed, and thus, the intensity of the electronic $\pi \rightarrow \pi^*$ transition may be affected. Frontier orbitals with the same symmetry as that found for the $[Cu(pds)_2]^-$ system[10] were also very recently reported for the neutral $[Ni(S_2C_2Me_2)_2]$.[27] In addition, short inter- and intraligand Se···Se distances are found for complexes **1**−**3** (see Table 5), indicating a considerable interaction between ligands as was observed in the $[Ni(S_2C_2Me_2)_2]$ complex and the Cu analogues. This situation explains the unusual reactivity of neutral $[Ni(S_2C_2Me_2)_2]$ with olefins that has led to some important applications,[28] which will be explored for our systems in the future.

**Table 5.** Average Inter- and Intraligand Se···Se Distances for Complexes **1**−**3**

| | 1 | 2 | 3 |
|---|---|---|---|
| interligand Se···Se | 3.186 | 3.188 | 3.194 |
| intraligand Se···Se | 3.291 | 3.317 | 3.310 |

Cyclic voltammograms for compounds **1**−**3** in $CH_3CN$ solutions are essentially the same, displaying an interesting but rather complicated redox behavior. If the voltage is maintained below +0.4 V, the compounds only show one reversible wave at $E_{1/2}$ = −0.12 V for **1** and $E_{1/2}$ = −0.16 V for **2** and **3**, which is assigned to the $Ni^{II}/Ni^{III}$ redox pair. The +0.04 V shift to higher values of the $Ni^{II}/Ni^{III}$ redox potential of **1** compared to **2** and **3** (see Figure 9) may account for the absence of alkaline sodium ions that interact with the pyrazine N atoms also in solution. However, if the applied potential is above +0.4 V, an irreversible oxidation wave is observed. This irreversible wave can be attributed to the formation of either the neutral complex $[Ni(pds)_2]$ or an unstable mixed-valence dimeric species.[23] More efforts will be devoted to work out the electrochemical processes

(24) (a) Mueller-Westerhoff, U. T., Vance, B.; Yoon, D. I. *Tetrahedron* **1991**, *47*, 909−932. (b) Bigoli, F.; Chen, C.-T.; Wu, W.-C.; Deplano, P.; Mercuri, M. L.; Pellinghelli, M. A.; Pilia, L.; Pintus, G.; Serpe, A.; Trogu, E. F. *Chem. Commun.* **2001**, 2246−2247.
(25) Drexhage, K. H.; Mueller-Westerhoff, U. T. *IEEE J. Quantum Electron.* **1972**, *QE-8*, 759. Drexhage, K. H.; Mueller-Westerhoff, U. T. U.S. Patent 3,743, 964, 1973.
(26) Tanaka, H.; Okano, Y.; Kobayashi, H.; Suzuki, W.; Kobayashi, A. *Science* **2001**, *291*, 285−287.
(27) Szilagyi, R. K.; Lim, B. S.; Glaser, T.; Holm, R. H.; Hedman, B.; Hodgson, K. O.; Solomon, E. I. *J. Am. Chem Soc.* **2003**, *125*, 9158−9169.
(28) Wang, K.; Stiefel, E. *Science* **2001**, *291*, 106−109.

operating on this system and to characterize the oxidized compounds obtained that may open the door to the synthesis of new conducting neutral complexes.

The $^1$H NMR and $^{13}$C NMR spectra of **1** were measured in DMSO-$d_6$, and only the signals corresponding to the $n$Bu$_4$N cations were observed. On the other hand, $^1$H NMR experiments in $CD_3CN$ are silent for **2** and **3**. This paramagnetic behavior was expected for **3**, since it is proposed as a paramagnetic Ni$^{III}$-d$^7$ species, but not for the square-planar diamagnetic Ni$^{II}$-d$^8$ compounds **1** and **2**. The $^1$H NMR spectrum for complex **2** was also measured in deuterated methanol with the same results. The EPR experiments, both in the solid state and in solution, shed light on these observations and allowed the understanding of this phenomenon.

The EPR spectrum of a polycrystalline sample of **3** is silent at room temperature, but a broad band appears at low temperatures: at 113 K a signal with $g = 2.093$ and $\Delta H_{pp} = 47$ G is observed, whereas in an acetone frozen solution at 77 K the signal splits into $g_1 = 2.109$ and $g_2 = 2.0627$ (see below for further assignments). On the other hand, the EPR spectrum of a polycrystalline sample of **2** in the temperature range 300−127 K is silent, in agreement with the square-planar structure of a diamagnetic Ni$^{II}$-d$^8$ species. However, a frozen acetonitrile solution of **2** at 127 K is truly EPR-active and shows an anisotropic signal with $g_1 = 2.235$ and $g_2 = 2.173$. The different behavior of **2** in solution compared to the solid state must be related to the coordination of solvent molecules to the Ni ion, clearly modifying the diamagnetic square-planar Ni$^{II}$ species in the solid state to a paramagnetic (distorted) octahedral geometry around the Ni$^{II}$. This solvent coordination effect is in agreement with the observed changes in the electronic spectra of these complexes by changing the solvent.

**Electrical and Magnetic Properties.** The electrical conductivity of **3** measured on a single crystal in the temperature range 160−360 K is shown in the Supporting Information (Figure S1). Compound **3** exhibits a semiconducting behavior with a low conductivity value at room temperature ($\sigma$(300 K) = 1.7 × 10$^{-4}$ S cm$^{-1}$) and an activation energy of 275.4 meV. The full ionic character and the regular stacking of the dimer units lead to a half-filled band structure, which in narrow-band molecular systems is invariably associated with a Mott−Hubbard insulating regime, in agreement with the low conductivity observed for this compound.

A bulk polycrystalline sample was used to measure the static magnetic susceptibility ($\chi_p$) of **3** versus temperature at 2 T in a Faraday balance (see the Supporting Information, Figure S2). The paramagnetic susceptibility was calculated from raw data considering a diamagnetic correction, estimated from tabulated Pascal constants as 1.9468 × 10$^{-4}$ emu mol$^{-1}$. Compound **3**, with two Ni$^{III}$ centers with $S = 1/2$, was expected to be paramagnetic. The measurements indicate that the paramagnetic susceptibility $\chi_p$ is on the order of 4 × 10$^{-4}$ emu mol$^{-1}$ at room temperature, remaining barely constant upon cooling to 50 K, where it becomes dominated by a Curie tail corresponding to approximately 1.5% of the $S = 1/2$ spins. A strong intradimer antiferromagnetic interaction should be expected from the intradimer distances found in the X-ray crystal structure. Indeed, the attempts to adjust the data to a singlet−triplet thermal excitation model[29] indicate a predominantly populated singlet state with an estimated $J \approx -1000$ K. Thus, the EPR signals at low temperature (see above) may correspond to isolated Ni$^{III}$ species associated with the Curie tail, rather than the triplet state for which there are no EPR data in dimers of Ni$^{III}$ species.[20] The study of the magnetic properties of **3** allows for the first time the comparison of the magnetic behavior of the dimeric bis(diselenolene)nickel(III) complex with that of the sulfur analogues. In [Ni(dcbdt)$_2$]$_2$($n$Bu$_4$N)$_2$ the antiferromagnetic coupling is weaker ($J = -447$ K).[20] This means that the substitution of S by Se accounts for a better Ni−Se orbital overlap in **3** and thus a more favorable antiferromagnetic exchange pathway. Other examples of weaker dimerized nickel(III) bis(dithiolene) complexes show indeed weaker antiferromagnetic interactions.[8]

## Summary

In this study we have shown that the two bis(diselenolene)-nickel(II) salts **1** and **2** present a completely different 3D structure as a consequence of the evident influence of the countercation used, which is in turn due to the side-coordination abilities of the pyrazine moieties of the pds ligand. In the context of the family of [M(L)$_2$]$^-$ (M = Cu, Ni; L = pds, pdt) compounds that we are studying,[9,10] the structure of **2** is an important achievement for the understanding of how the system accommodates two sodium cations per complex dianion, resulting in a puzzling array of orthogonal layers with a very interesting and novel coordination environment for the Na ions.

Furthermore, to the best of our knowledge, **3** exhibits the first structure of a bis(diselenolene)nickel(III) dimer arranged in segregated stacks of dimers. Although possessing a structure dimerized similarly to that of the bis(dichalcogenene)-nickel(III) compounds [Ni(dsit)$_2$]$_2$($n$Bu$_4$N)$_2$[21] and [Ni(dcbdt)$_2$]$_2$-($n$Bu$_4$N)$_2$,[20] the Na coordination to the pyrazine moieties in **3** allows the formation of stacks of dimers in a different manner. Therefore, we show that the alkaline side coordination is a key strategy for the crystal engineering of novel compounds with interesting or even desired physical properties.

From the point of view of the electronic description of these systems, the pds ligand in complexes **1**−**3** does not play an active role in the redox processes as deduced from the structural data, as similarly concluded for the Cu analogues.[10] Thus, a metal-centered Ni$^{II}$/Ni$^{III}$ redox process is proposed to occur, which is clearly reflected in the geometry change that accompanies the alteration of the Ni center oxidation state.

**Acknowledgment.** This work was supported by grants from DGI Spain (Project BQU2003-00760), DGR Catalonia (Project 2001SGR00362), and FCT Portugal (Contract POCTI/35342/QUI/2000). The collaboration between the

(29) Carlin, R. L. *Magnetochemistry*; Springler-Verlag: Heidelberg, Germany, 1986.

team authors from Barcelona and Sacavém was supported by the ICCT-CSIC bilateral agreement and benefited also from COST action D14. We thank E. B. Lopes for electrical conductivity measurements.

**Supporting Information Available:** Complete X-ray crystallographic data for **1**−**3** (CIF format) and further structural details of complexes **1**−**3** and electrical conductivity and magnetic susceptibility measurements on compound **3** (PDF). This material is available free of charge via the Internet at http://pubs.acs.org.

IC049860X